Optical Engineering

SPIEDigitalLibrary.org/oe

Fractional domain varying-order differential denoising method

Yan-Shan Zhang
Feng Zhang
Bing-Zhao Li
Ran Tao

SPIE

Fractional domain varying-order differential denoising method

Yan-Shan Zhang,[a] Feng Zhang,[b] Bing-Zhao Li,[a] and Ran Tao[a,b,*]
[a]Beijing Institute of Technology, Department of Mathematics, Beijing 100081, China
[b]Beijing Institute of Technology, Department of Electronic Engineering, Beijing 100081, China

Abstract. Removal of noise is an important step in the image restoration process, and it remains a challenging problem in image processing. Denoising is a process used to remove the noise from the corrupted image, while retaining the edges and other detailed features as much as possible. Recently, denoising in the fractional domain is a hot research topic. The fractional-order anisotropic diffusion method can bring a less blocky effect and preserve edges in image denoising, a method that has received much interest in the literature. Based on this method, we propose a new method for image denoising, in which fractional-varying-order differential, rather than constant-order differential, is used. The theoretical analysis and experimental results show that compared with the state-of-the-art fractional-order anisotropic diffusion method, the proposed fractional-varying-order differential denoising model can preserve structure and texture well, while quickly removing noise, and yields good visual effects and better peak signal-to-noise ratio. [DOI: 10.1117/1.OE.53.10.102102]

Keywords: image processing; denoising; fractional; anisotropic diffusion; varying-order differential.

Paper 131739SS received Nov. 13, 2013; revised manuscript received Jan. 17, 2014; accepted for publication Feb. 3, 2014; published online Apr. 15, 2014.

1 Introduction

Digital images play an important role in many applications, such as astronomy, computer tomography, machine vision, and geographical information systems. In practice, an image is mixed with a certain level of noise which decreases the visual quality. Therefore, removal of the noise is a common problem in image processing. An image gets corrupted with noise during acquisition or transmission due to channel errors or faulty hardware. Removing noise from noisy images is still a challenging problem for researchers.

Denoising, as the word suggests, is the removal of noisy components from the pixels of an image. Lots of research has been concentrated on this area for a long time, and many methodologies have been proposed by researchers for achieving good performance,[1–6] in which partial differential equation (PDE)-based image processing techniques offer great potential in developing image denoising applications with good results. However, these conventional PDE-based models might lose interesting fine structures during the denoising process. As a consequence, many other PDE-based denoising models have been proposed, and have had much success in preserving structures, while removing noise. Based on the work of Perona and Malik,[7] which replaces the isotropic diffusion by anisotropic diffusion, many methods connecting adaptive smoothing with systems of nonlinear PDE[8–13] have been proposed to preserve important structures in images, while removing noise. Anisotropic diffusion is associated with an energy-dissipating process that seeks the minimum of the energy functional. When the energy functional is the total variation (TV) norm of the image, the well-known TV minimization model[14] can be obtained.

Although these techniques have been demonstrated to achieve a good tradeoff between noise removal and edge preservation, the recovered images by using these denoising techniques are often piecewise constant. Thus, the finer details in the original image may not be recovered satisfactorily and affine regions will look "blocky."

To reduce the blocky effect, while preserving sharp jump discontinuities (edges), many other nonlinear filters have been suggested in the literature.[15–20] During the last few years, fourth-oder PDEs have been of a special interest.[18–20] For example, You and Kaveh proposed a class of fourth-order PDEs which are Euler–Lagrange equations of a cost functional making an increasing function of the absolute value of the Laplacian of the image intensity function.[19] Piecewise planar images look more natural than the step images that are stationary points of second-order PDEs.

The fractional-order PDE is an important branch of the PDEs. Cuesta proposed fractional-order linear integral–differential equations, which interpolated heat equations and wave equations using the Riemann–Liouville(R–L) fractional derivative.[21] Mathieu et al. used fractional derivative to detect the image edges.[22] Pu et al. designed the fractional derivative filter to detect the texture details of images.[23] Zhang et al. introduced fractional-order image inpainting into metal artifacts reduction in computed tomography (CT) images.[24] Bai and Feng derived the fractional-order anisotropic diffusion model, and they found that the optimal performance can be achieved when the order was 1.2 or 1.8.[25] However, all above works use the same differential order for a whole image. Then an interesting question has arisen: can we use different differential orders for a whole image at the same time? To the best of our knowledge,

*Address all correspondence to: Ran Tao, E-mail: rantao@bit.edu.cn

there are no such published papers which have considered this issue. Therefore, it is interesting and worthwhile to investigate this topic in detail.

In this article, we propose a new image-denoising method (named fractional-varying-order differential model). In this model, differential orders can vary with the gradient of an image so that the multiple differential can be used in a whole image at the same time. Thus, the blocky effect can be suppressed and the texture will not be smoothed out just as another high frequency noise, while removing noise.

The outline of this article is as follows. In Sec. 2, we will propose the concept of fractional-varying-order differential. In Sec. 3, the denoising model based on fractional-varying-order differential will be established. In Sec. 4, we will show some simulation results. And the conclusion will be made in Sec. 5.

2 Methodology

2.1 *Traditional Constant-Order Differential*

Definition 2.1. Supposing $\vec{d}(t)=[d_1(t),d_2(t),\cdots,d_n(t)]^T$ is a $n\times 1$ function vector, $u(x,y)=[u_{ij}(x,y)]_{n\times m}$ is a $n\times m$ function matrix. D_α is αth ($\alpha\in R^+$) fractional derivative operator, then we have the following results:

$$\vec{f}^{(\alpha)}(t):=[f_1^{(\alpha)}(t),f_2^{(\alpha)}(t),\cdots,f_n^{(\alpha)}(t)]^T, \tag{1}$$

$$D_\alpha u(x,y) := \begin{pmatrix} D_\alpha u_{11}(x,y) & D_\alpha u_{12}(x,y) & \cdots & D_\alpha u_{1\,m}(x,y) \\ D_\alpha u_{21}(x,y) & D_\alpha u_{22}(x,y) & \cdots & D_\alpha u_{2\,m}(x,y) \\ \vdots & \vdots & \ddots & \vdots \\ D_\alpha u_{n1}(x,y) & D_\alpha u_{n2}(x,y) & \cdots & D_\alpha u_{nm}(x,y) \end{pmatrix}. \tag{2}$$

The previous image processing methods based on differential use a constant-order differential, which is the same differential order for a whole image. According to the theory of fractional-order differential in the application of digital image processing, using different differential orders to process an image will produce different effects. Thus, we put forward the concept of varying-order differential, namely, when an image is processed by differential, the differential orders of different parts of the image can be variable.

2.2 *Proposed Fractional-Varying-Order Differential*

Definition 2.2. Supposing $\vec{d}(t)=[d_1(t),d_2(t),\cdots,d_n(t)]^T$ is a $n\times 1$ vector, $\vec{f}(t):=[f_1(t),f_2(t),\cdots,f_n(t)]^T$ is a $n\times 1$ function vector, $\mathbf{A}=(a_{ij})_{n\times m}$ is a $n\times m$ matrix and $\mathbf{u}(x,y)=[u_{ij}(x,y)]_{n\times m}$ is a $n\times m$ function matrix. D_α is αth ($\alpha\in R^+$) fractional derivative operator, then we define:

$$\vec{d}^{\mathbf{A}}:=\begin{pmatrix} d_1^{a_{11}} & d_1^{a_{12}} & \cdots & d_1^{a_{1\,m}} \\ d_2^{a_{21}} & d_2^{a_{22}} & \cdots & d_2^{a_{2\,m}} \\ \vdots & \vdots & \ddots & \vdots \\ d_n^{a_{n1}} & d_n^{a_{n2}} & \cdots & d_n^{a_{nm}} \end{pmatrix},$$

$$\vec{f}^{(\mathbf{A})}(t):=\begin{pmatrix} f_1^{(a_{11})}(t) & f_1^{(a_{12})}(t) & \cdots & f_1^{(a_{1\,m})}(t) \\ f_2^{(a_{21})}(t) & f_2^{(a_{22})}(t) & \cdots & f_2^{(a_{2\,m})}(t) \\ \vdots & \vdots & \ddots & \vdots \\ f_n^{(a_{n1})}(t) & f_n^{(a_{n2})}(t) & \cdots & f_n^{(a_{nm})}(t) \end{pmatrix},$$

$$D_{\mathbf{A}}:=\begin{pmatrix} D_{a_{11}} & D_{a_{12}} & \cdots & D_{a_{1\,m}} \\ D_{a_{21}} & D_{a_{22}} & \cdots & D_{a_{2\,m}} \\ \vdots & \vdots & \ddots & \vdots \\ D_{a_{n1}} & D_{a_{n2}} & \cdots & D_{a_{nm}} \end{pmatrix},$$

$$D_{\mathbf{A}}\mathbf{u}(x,y) := \begin{pmatrix} D_{a_{11}}u_{11}(x,y) & D_{a_{12}}u_{12}(x,y) & \cdots & D_{a_{1\,m}}u_{1\,m}(x,y) \\ D_{a_{21}}u_{21}(x,y) & D_{a_{22}}u_{22}(x,y) & \cdots & D_{a_{2\,m}}u_{2\,m}(x,y) \\ \vdots & \vdots & \ddots & \vdots \\ D_{a_{n1}}u_{n1}(x,y) & D_{a_{n2}}u_{n2}(x,y) & \cdots & D_{a_{nm}}u_{nm}(x,y) \end{pmatrix}, \tag{3}$$

we call $D_{\mathbf{A}}$ as fractional-varying-order differential operator.

Thus, we define the fractional-varying-order derivative in the frequency domain as

$$D_{\vec{\alpha}}f(t)\leftrightarrow(j\vec{\omega})^{\vec{\alpha}}\hat{f}(\vec{\omega}), \tag{4}$$

where $\vec{\alpha}$ is an appropriate vector. It is obvious that the semigroup property of fractional-varying-order derivative operators holds, namely

$$(D_{\vec{\alpha}})(D_{\vec{\beta}})f=(D_{\vec{\beta}})(D_{\vec{\alpha}})f=(D_{\vec{\alpha}+\vec{\beta}})f, \tag{5}$$

where vectors $\vec{\alpha},\vec{\beta}$ have the same dimension.

For any $g(x,y)\in L^2(R^2)$, the corresponding two-dimensional (2-D) Fourier transform is

$$\hat{g}(\omega_1,\omega_2)=\int_R g(x,y)\exp[-j(\omega_1 x+\omega_2 y)]\mathrm{d}x\mathrm{d}y. \tag{6}$$

Thus, the corresponding fractional-varying-order partial derivatives are

$$D_{\mathbf{A}x}g=F^{-1}[(j\omega_1)^{\mathbf{A}}\hat{g}(\omega_1,\omega_2)] \tag{7}$$

and

$$D_{\mathbf{A}y}g=F^{-1}[(j\omega_2)^{\mathbf{A}}\hat{g}(\omega_1,\omega_2)], \tag{8}$$

where $\mathbf{A}$ is a $n\times m$ matrix, F^{-1} is an inverse 2-D Fourier transform operator.

3 Proposed Approach

3.1 *Fractional-Varying-Order Differential Denoising Model*

Smoothing by local-weighted averaging is an effective image regularization method that has been used for denoising, restoration, and enhancement. A drawback is that smoothing can damage image features, such as edges, lines, and textures. To avoid the damage, the smoothing has to be adaptively controled by the amount or the direction of smoothing. A classic example of adaptive smoothing is the anisotropic diffusion scheme of Perona and Malik,[7] in which the smoothing process is formulated by a PDE. Let t denotes the time and $c(\cdot)$ be the diffusion coefficient, the anisotropic diffusion as formulated in Ref. 7 can be presented as

$$\frac{\partial u}{\partial t} = \mathrm{div}[c(|\nabla u|^2)\nabla u]. \tag{9}$$

This equation is associated with the following energy functional:

$$E(u) = \int_\Omega f(|\nabla u|)\mathrm{d}\Omega, \tag{10}$$

where Ω is the image support, and $f(\cdot) \geq 0$ is an increasing function associated with the diffusion coefficient

$$c(s) = \frac{f'(\sqrt{s})}{\sqrt{s}}. \tag{11}$$

Anisotropic diffusion is then shown to be an energy-dissipating process that seeks the minimum of the energy functional. We consider the following functional defined in the space of continuous images over a support of Ω. This equation is associated with the following energy functional:

$$E(u) = \int_\Omega f(|D_{\mathbf{A}}u|)\mathrm{d}\Omega, \tag{12}$$

where $\mathbf{A} = \alpha(|\nabla u|)$ and $\alpha(\cdot)$ is an increasing function and meets the condition

$$\alpha(x) \to \begin{cases} 1, & x \to 0 \\ 2, & x \to \infty \end{cases}.$$

$D_{\mathbf{A}}$ denotes the fractional-varying-order differential operator defined by $D_{\mathbf{A}}u = (D_{\mathbf{A}x}u, D_{\mathbf{A}y}u)$ and $|D_{\mathbf{A}}u| = \sqrt{D_{\mathbf{A}x}^2 + D_{\mathbf{A}y}^2}$. We can formally compute the Euler–Lagrange equation for this minimization problem as follows. Take any test function $\eta \in C^\infty(\Omega)$ and assume

$$\Phi(a) = \int_\Omega f(|D_{\mathbf{A}}u + aD_{\mathbf{A}}\eta|)\mathrm{d}x\mathrm{d}y. \tag{13}$$

We obtain

$$\begin{aligned}\Phi'(0) &= \frac{d}{da}\int_\Omega f(|D_{\mathbf{A}}u + aD_{\mathbf{A}}\eta|)\mathrm{d}x\mathrm{d}y|_{a=0} \\ &= \int_\Omega \left[f'(|D_{\mathbf{A}}u|)\frac{D_{\mathbf{A}x}u}{|D_{\mathbf{A}}u|}D_{\mathbf{A}x}\eta + f'(|D_{\mathbf{A}}u|)\frac{D_{\mathbf{A}y}u}{|D_{\mathbf{A}}u|}D_{\mathbf{A}y}\eta\right]\mathrm{d}x\mathrm{d}y \\ &= \int_\Omega (D_{\mathbf{A}x}^*[c(|D_{\mathbf{A}}u|^2)D_{\mathbf{A}x}u] + D_{\mathbf{A}y}^*[c(|D_{\mathbf{A}}u|^2)D_{\mathbf{A}y}u)]\eta\mathrm{d}x\mathrm{d}y\end{aligned}$$

for all $\eta \in C^\infty(\Omega)$, where $D_{\mathbf{A}x}^*$ is the adjoint of $D_{\mathbf{A}x}$ and $D_{\mathbf{A}y}^*$ is the adjoint of $D_{\mathbf{A}y}$, respectively. Thus, the Euler–Lagrange equation is

$$D_{\mathbf{A}x}^*[c(|D_{\mathbf{A}}u|^2)D_{\mathbf{A}x}u] + D_{\mathbf{A}y}^*[c(|D_{\mathbf{A}}u|^2)D_{\mathbf{A}y}u] = 0. \tag{14}$$

The Euler–Lagrange equation may be solved through the following gradient descent procedure:

$$\frac{\partial u}{\partial t} = -D_{\mathbf{A}x}^*[c(|D_{\mathbf{A}}u|^2)D_{\mathbf{A}x}u] - D_{\mathbf{A}y}^*[c(|D_{\mathbf{A}}u|^2)D_{\mathbf{A}y}u] \tag{15}$$

with the observed image as the initial condition. The solution is arrived when $t \to \infty$, but the time evolution may be stopped earlier to achieve an optimal tradeoff between noise removal and edge preservation.

3.2 *Analysis of the New Model*

For any function $f(t) \in L^2(R)$, the Fourier transform is

$$\hat{f}(\omega) = \int_R f(t)\exp(-j\omega t)\mathrm{d}t. \tag{16}$$

The equivalent form of the kth-order ($k \in Z^+$) derivative in the frequency domain is

$$(D_k\hat{f})(\omega) = (j\omega)^k\hat{f}(\omega) = \hat{d}_k(\omega)\hat{f}(\omega). \tag{17}$$

Similarly, the equivalent form of the αth-order ($\alpha \in R^+$) derivative in the frequency domain is

$$(D_\alpha f)(\omega) = (j\omega)^\alpha\hat{f}(\omega) = \hat{d}_\alpha(\omega)\hat{f}(\omega), \tag{18}$$

where $\hat{d}_\alpha(\omega) = (j\omega)^\alpha$ is called as α'th-order differential multiplier-function. Its complex exponential form and time domain form are

$$\begin{cases} \hat{d}_\alpha(\omega) = \hat{a}_\alpha(\omega)\exp[j\theta_\alpha(\omega)] \\ \hat{a}_\alpha(\omega) = |\omega|^\alpha, \theta_\alpha(\omega) = \frac{\alpha\pi}{2}\mathrm{sgn}(\omega) \end{cases}. \tag{19}$$

From Eq. (19), we can obtain the amplitude–frequency curves of fractional-order differential, as shown in Fig. 1, from which we find that the fractional-order differential can improve the high-frequency components of a signal in meantime nonlinearly preserve the low-frequency components of the signal.

Considering the feature of the fractional-order differential for the signal, the fractional-varying-order differential model is proposed. In the past, the differential orders used to

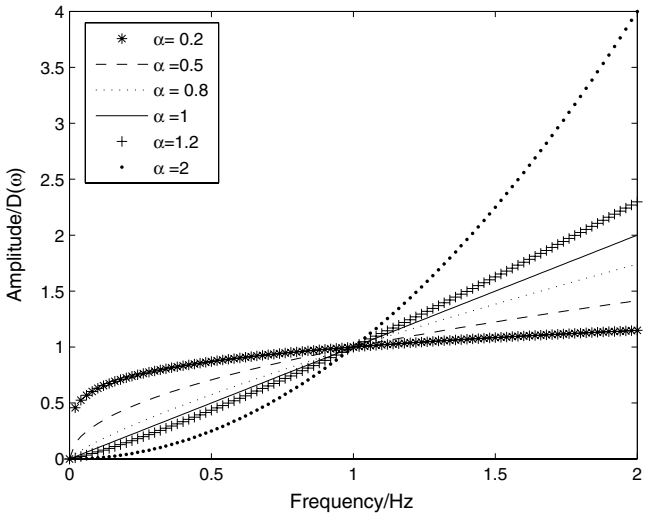

Fig. 1 The amplitude–frequency curve of fractional-order differential.

process different parts of an image are the same. However, in our model, the differential orders are different and are determined by the value of gradient modulus of the image. For example, when the pixel is located in smooth image area, the image gradient is very small and it cause the differential order α to be close to 1. This phenomenon is beneficial for denoising and suppressing the "staircasing" effect. Conversely, when the pixel is located in image edges, the image gradient is large, and the differential order α should be a little larger value. This will preserve important texture.

Note that in the proposed Euler–Lagrange equation, when $\mathbf{A} = 1_E$ (a matrix of ones where every element is equal to one), Eq. (15) is equivalent to the Perona–Malik equation shown in Eq. (9); when $\mathbf{A} = 2 \cdot 1_E$, Eq. (15) is equivalent to the fourth-order anisotropic diffusion equation in Ref. 19.

4 Numerical Implementation and Simulation Results

In this section, we will verify our proposed image-denoising model considered in the previous section. To analyze the performance of our model, we compare our model with fractional-order anisotropic diffusion model. The restoration

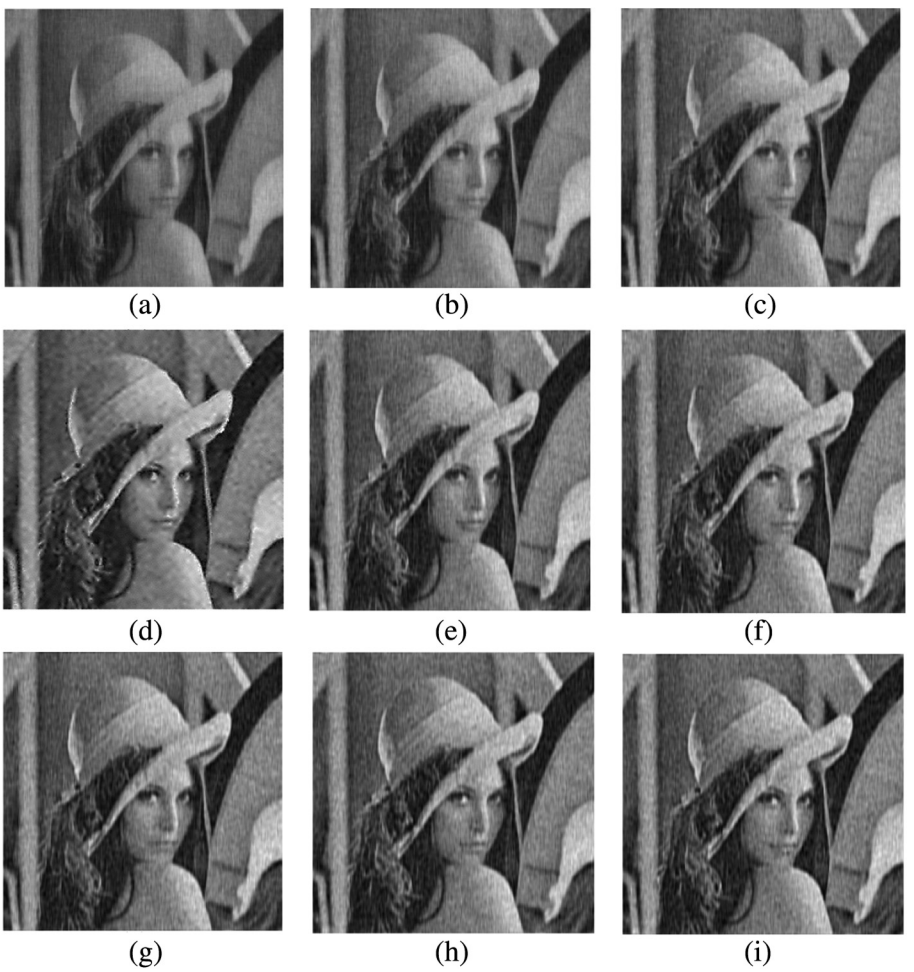

Fig. 2 Comparison of denoising results with different α in the case of additive Gaussian white noise ($\sigma = 25$). (a) $\alpha = 0.4$, PSNR = 22.8606; (b) $\alpha = 0.6$, PSNR = 25.8644; (c) $\alpha = 0.8$, PSNR = 26.4067; (d) $\alpha = 1$, PSNR = 26.4877; (e) $\alpha = 1.2$, PSNR = 26.4880; (f) $\alpha = 1.4$, PSNR = 26.3514; (g) $\alpha = 1.6$, PSNR = 26.2974; (h) $\alpha = 1.8$, PSNR = 26.1748; (i) $\alpha = 2$, PSNR = 26.1688.

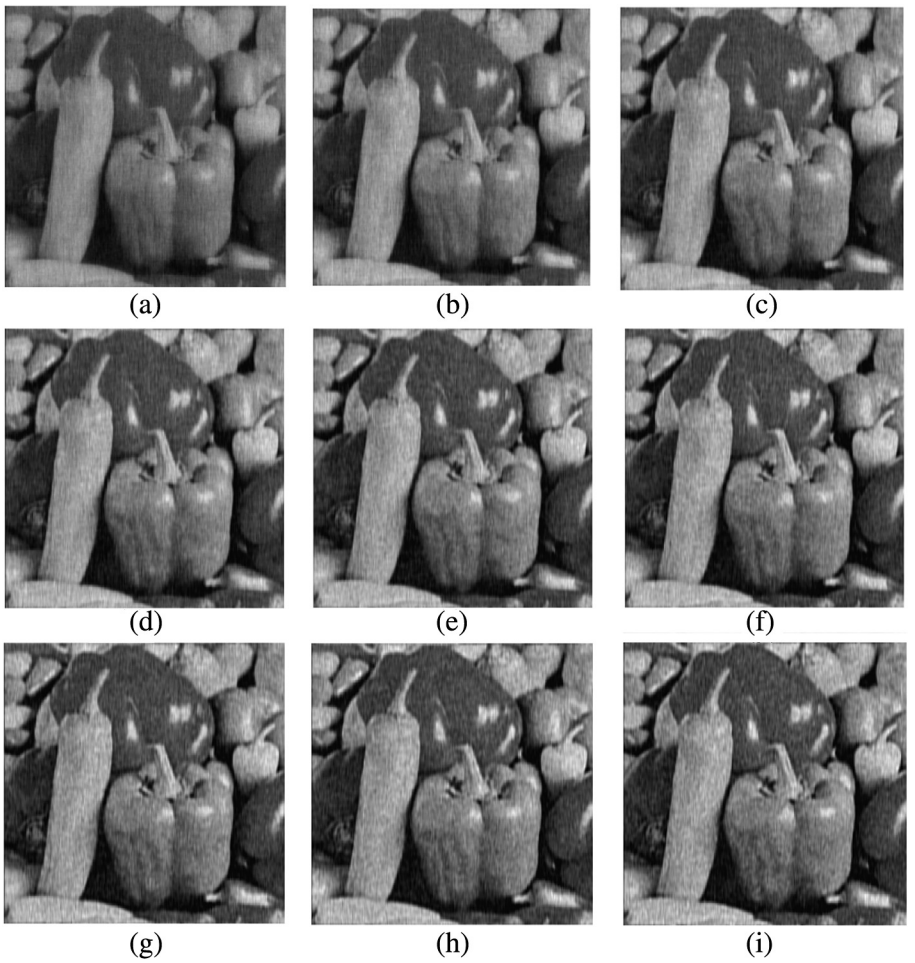

Fig. 3 Comparison of denoising results with different α in the case of additive Gaussian white noise ($\sigma = 25$). (a) $\alpha = 0.4$, PSNR = 22.3164; (b) $\alpha = 0.6$, PSNR = 25.5216; (c) $\alpha = 0.8$, PSNR = 26.3960; (d) $\alpha = 1$, PSNR = 26.5783; (e) $\alpha = 1.2$, PSNR = 26.5872; (f) $\alpha = 1.4$, PSNR = 26.5234; (g) $\alpha = 1.6$, PSNR = 26.3542; (h) $\alpha = 1.8$, PSNR = 26.3499; (i) $\alpha = 2$, PSNR = 26.2076.

quality is measured by the peak signal-to-noise ratio (PSNR), which is defined as

$$\mathrm{PSNR} = 10 \times \log_{10}\left(\frac{255^2}{\mathrm{MSE}}\right),$$

where $\mathrm{MSE} = \|u - u_0\|_2^2/(M \times N)$ is the mean-squared error, u_0 is the original image, u denotes the recovered image, and the unit of PSNR is decibel. The larger the value of PSNR is, the better the performance is. The test 256×256 grayscale images include Lena and Peppers.

To summarize, our noise removal approach is realized by the following steps:

(1) Let the input image be u and set $n = 1$, $u_n = u, k, \Delta t, t = k\Delta t$, compute the 2-D DFT $\hat{u}_n$ of u_n.

(2) Compute $|\nabla u_n|, \mathbf{A} = 2 \cdot (|\nabla u_n| + 1)/(|\nabla u_n| + 2)$.

(3) Compute $\mathbf{A}$-order partial differences $\tilde{D}_{\mathbf{A}x}u_n$ and $\tilde{D}_{\mathbf{A}y}u_n$ by the formula:

$$\tilde{D}_{\mathbf{A}x}u_n = F^{-1}\{[1 - \exp(-j2\pi\omega_1/m)]^{\mathbf{A}} \exp \times (j\pi\mathbf{A}\omega_1/m)F(u_n)\}$$

and

$$\tilde{D}_{\mathbf{A}y}u_n = F^{-1}\{[1 - \exp(-j2\pi\omega_2/m)]^{\mathbf{A}} \exp \times (j\pi\mathbf{A}\omega_2/m)F(u_n)\},$$

compute $K_1^* = \mathrm{diag}(\mathrm{conj}\{[1 - \exp(-j2\pi\omega_1/m)]^{\mathbf{A}} \exp(j\pi\mathbf{A}\omega_1/m)\})$, and $K_2^* = \mathrm{diag}(\mathrm{conj}\{[1 - \exp(-j2\pi\omega_2/m)]^{\mathbf{A}} \exp(j\pi\mathbf{A}\omega_2/m)\})$.

(4) Compute $h_{xn} = c(|\tilde{D}_{\mathbf{A}}u_n|^2)\tilde{D}_{\mathbf{A}x}u_n$ and $h_{yn} = c(|\tilde{D}_{\mathbf{A}}u_n|^2)\tilde{D}_{\mathbf{A}y}u_n$, then compute $\hat{g}_n = K_1^* \circ \mathrm{F}(h_x n) + K_2^* \circ \mathrm{F}(h_y n)$.

(5) Compute $\hat{u}_{n+1} = \hat{u}_n - \hat{g}_n \cdot \Delta t$ and set $n = n + 1$; if $n = k$, compute the 2-D IDFT of $\hat{u}_n$, stop; else go to (2).

In our experiments, we take $\Delta t = 0.05$ and $k = 55$, and use the following function[26]

$$c(s) = \frac{1}{1 + (s/b)^2}$$

with $b = 10$ in our experiment results.

In Figs. 2 and 3, we separately list denoised Lena and Peppers images using fractional-order anisotropic diffusion

Fig. 4 Comparison of denoising results by using fractional-order Perona and Malik (PM) model and our proposed model on Lena. (a) Original image; (b) Damaged image with $\sigma = 25$ Gaussian noise (PSNR = 20.1500); (c) fractional-order anisotropic diffusion model (PSNR = 26.4880, $\alpha = 1.2$); (d) Our proposed model (PSNR = 27.4676).

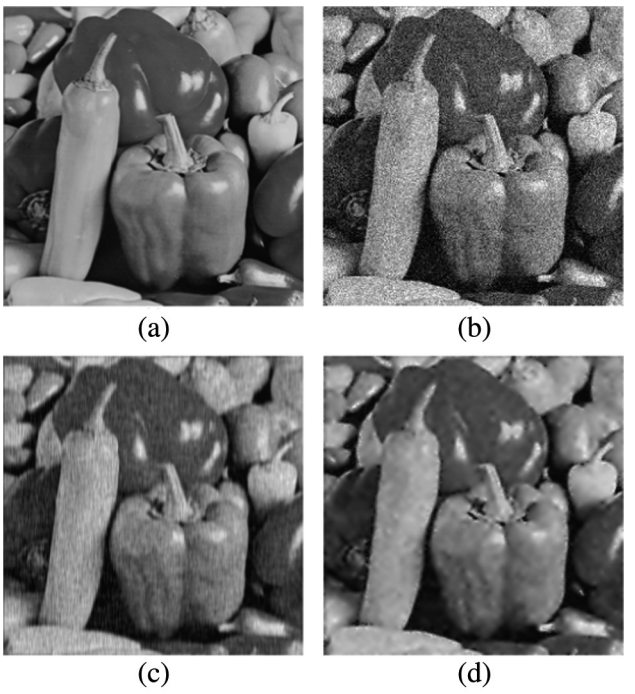

Fig. 5 Denoising results of comparison of fractional-order anisotropic diffusion model and our proposed model on Peppers. (a) Original image; (b) Damaged image with $\sigma = 25$ Gaussian noise (PSNR = 20.1379); (c) fractional-order anisotropic diffusion model (PSNR = 26.5872, $\alpha = 1.2$); (d) Our proposed model (PSNR = 28.0319).

model with different fractional orders α. It can be observed that the PSNR reaches a maximum at $\alpha = 1.2$. Figures. 4 and 5 show the results of noise removal on Lena and Peppers using our proposed model and the original fractional-order anisotropic diffusion model. Figures 4(a) and 5(a) are the original images of the Lena and Peppers; Figs. 4(b) and 5(b) are damaged images of the Lena and Peppers with $\sigma = 25$ Gaussian noise, and the corresponding PSNRs are 20.1500 and 20.1379, respectively. Figures 4(c) and 5(c) are the results of using fractional-order anisotropic diffusion model with $\alpha = 1.2$, and the PSNRs are 26.4880 and 26.5872, respectively. Although using our model, the PSNRs reach 27.4676 and 28.0319, respectively [see Figs. 4(d) and 5(d)]. From Figs. 2 to 5, we can find that our proposed model is better than the original fractional-order anisotropic diffusion model with respect to visual effect and the PSNR.

5 Conclusion

In this article, we have proposed a fractional-varying-order differential model for image denoising. The model can adaptively select the differential order according to the value of noise visibility of each pixel, which can effectively avoid staircase effect and the difficulties in parameter selection. In addition, this method is very easy to perform. It is a new idea of adaptive image processing. The experiment results show that this method is able to achieve a good effect in the respect of noise removal and edge preservation during the process of image smoothing. Future works involve extending the proposed method to other PDEs and variational models.

Acknowledgments

This work was supported in part by the National Natural Science Foundation of China under Grants No. 61331021 and No. 61201354, by the Beijing Higher Education Young Elite Teacher Project, by the Basic Science Foundation of Beijing Institute of Technology under Grant 20120542005, by Program for New Century Excellent Talents in University No. NCET-12-0042 and by the National Key Basic Research Program founded by MOST under Grant 2010CB731902.

References

1. X. Y. Zeng and L. H. Yang, "Mixed impulse and Gaussian noise removal using detail-preserving regularization," *Opt. Eng.* **49**(9), 097002 (2010).
2. S. H. Lee and J. K. Seo, "Noise removal with Gauss curvature-driven diffusion," *IEEE Trans. Image Process.* **14**(7), 904–909 (2005).
3. G. N. Chen et al., "Biomedical images texture detail denosing based on PDE," *Proc. SPIE* **7519**, 75190A (2009).
4. K. Chen, "Adaptive smoothing via contextual and local discontinuities," *IEEE Trans. Pattern Anal. Mach. Intell.* **27**(10), 1552–1567 (2005).
5. C. Jung et al., "Spatial-gradient-local-inhomogeneity: an efficient image denoising prior," *J. Electron. Imaging* **19**(3), 033005 (2010).
6. Y. H. Guo and H. D. Cheng, "Image noise removal approach based on subpixel anisotropic diffusion," *J. Electron. Imaging* **21**(3), 033026 (2012).
7. P. Perona and J. Malik, "Scale-space and edge detection using anisotropic diffusion," *IEEE Trans. Pattern Anal. Mach. Intell.* **12**(7), 629–639 (1990).
8. F. Catte et al., "Image selective smoothing and edge detection by nonlinear diffusion," *SIAM J. Numer. Anal.* **29**(1), 182–193 (1992).
9. R. A. Carmona and S. Zhong, "Adaptive smoothing respecting feature directions," *IEEE Trans. Image Process.* **7**(3), 353–358 (1998).
10. J. Monteil and A. Beghdadi, "A new interpretation and improvement of the nonlinear anistropic diffusion for image enhancement," *IEEE Trans. Pattern Anal. Mach. Intell.* **21**(9), 940–946 (1999).
11. A. K. Mandava and E. E. Regentova, "Image denoising based on adaptive nonlinear diffusion in wavelet domain," *J. Electron. Imaging* **20**(3), 033016 (2011).

12. A. C. C. Shih, H. Y. M. Liao, and C. S. Lu, "A new iterated two-band diffusion equation: theory and its application," *IEEE Trans. Image Process.* **12**(4), 466–476 (2003).
13. Y. Wang et al., "Region-based adaptive anisotropic diffusion for image enhancement and denoising," *Opt. Eng.* **49**(11), 117007 (2010).
14. L. I. Rudin, S. Osher, and E. Fatemi, "Nonlinear total variation based noise removal algorithms," *Physica D* **60**(1), 259–268 (1992).
15. G. M. Cui et al., "Multi scale detail-preserving denoising method of infrared image via relative total variation," *Proc. SPIE* **8907**, 890713 (2013).
16. R. Tao, H. Wan, and Y. Wang, "Artifact-free despeckling of SAR images using contourlet," *IEEE Geosci. Remote Sens. Lett.* **9**(5), 980–984 (2012).
17. T. F. Chan, A. Marquina, and P. Mulet, "High-order total variationbased image restoration," *SIAM J. Sci. Comput.* **22**(2), 503–516 (2000).
18. B. B. Lu and Q. Liu, "Image restoration with surface-based fourth order partial differential equation," *Proc. SPIE* **7744**, 774424 (2010).
19. Y. L. You and M. Kaveh, "Fourth-order partial differential equations for noise removal," *IEEE Trans. Image Process.* **9**(10), 1723–1730 (2000).
20. M. Lysaker, A. Lundervold, and X. C. Tai, "Noise removal using fourth-order partial differential equation with applications to medical magnetic resonance images in space and time," *IEEE Trans. Image Process.* **12**(12), 1579–1590 (2003).
21. E. Cuesta and J. F. Codes, "Image processing by means of a linear integro-differential equation," in *Proc. 3rd IASTED Int. Conf. Visualization, Imaging, Image Process.*, pp. 438–442, ACTA Press, Calgary, Alberta, Canada (2003).
22. B. Mathieu et al., "Fractional differentiation for edge detection," *Signal Process.* **83**(11), 2421–2432 (2003).
23. Y. F. Pu et al., "Fractional differential approach to detecting textural features of digital image and its fractional differential filter implementation," *Sci. China Ser. F: Inform. Sci.* **51**(9), 1319–1339 (2008).
24. Y. Zhang et al., "A new CT metal artifacts reduction algorithm based on fractional-order sonogram inpainting," *J. X-ray Sci. Technol.* **19**(3), 373–384 (2011).
25. J. Bai and X. C. Feng, "Fractional-order anisotropic diffusion for image denoising," *IEEE Trans. Image Process.* **16**(10), 2492–2502 (2007).
26. B. M. H. Romeny, *Geometry-Driven Diffusion in Computer Vision*, Kluwer academic, Norwell, Massachusetts (1994).

Yan-Shan Zhang received his BS degree in mathematics from Zhengzhou Institute of Aeronautical Industry Management, Zhengzhou, China, in 2010. He is currently pursuing his PhD degree in mathematics at Beijing Institute of Technology, Beijing, China. His research interests include digital image processing, fractional Fourier transform, and fractional calculus.

Feng Zhang received his BS and MS degrees in communication and information systems from Zhengzhou University, Zhengzhou, China, in 2003 and 2006, and a PhD in information and communication engineering from Beijing Institute of Technology, Beijing, China, in 2010, respectively. Presently, he is a lecturer with the Department of Electronic Engineering, Beijing Institute of Technology. His research interests include time-frequency analysis and radar signal processing.

Bing-Zhao Li received his BS degree in mathematics from Shandong Normal University, Jinan, China, in 1998 and his MS and PhD degrees from the Beijing Institute of Technology, Beijing, China, in 2001 and 2007, respectively. Presently, he is an associate professor with the Department of Mathematics. His research interests include time-frequency analysis, digital signal processing, and image processing.

Ran Tao received a PhD degree in electrical engineering from Harbin Institute of Technology, Harbin, in 1993. He has been a professor at Beijing Institute of Technology since 1999. His research interests include fractional Fourier transform with applications in radar and communication systems. He is the vice president of Chinese Radar Industry Association, and a Fellow of the Chinese Institute of Electronics.